## REFERENCES


1 Jackson KA, Majka SM, Wang H et al. Regeneration of ischemic cardiac muscle and vascular endothelium by adult stem cells. J Clin Invest 2001;107:1395–1402.

2 Orlic D, Kajstura J, Chimenti S et al. Bone marrow cells regenerate infarcted myocardium. Nature 2001;410:701–705.

3 LaBarge MA, Blau HM. Biological progression from adult bone marrow to mononucleate muscle stem cell to multinucleate muscle fiber in response to injury. Cell 2002;111:589–601.

4 Harris RG, Herzog EL, Bruscia EM et al. Lack of a fusion requirement for development of bone marrow-derived epithelia. Science 2004;305:90–93.

5 Brittan M, Braun KM, Reynolds LE et al. Bone marrow cells engraft within the epidermis and proliferate in vivo with no evidence of cell fusion. J Pathol 2005;205:1–13.

6 Houghton J, Stoicov C, Nomura S et al. Gastric Cancer Originating from Bone Marrow-Derived Cells. Science 2004;306:1568–1571.

7 Borue X, Lee S, Grove J et al. Bone marrow-derived cells contribute to epithelial engraftment during wound healing. Am J Pathol 2004;165:1767–1772.

8 Kollet O, Shivtiel S, Chen YQ et al. HGF, SDF-1, and MMP-9 are involved in stress-induced human $CD34^{+}$ stem cell recruitment to the liver. J Clin Invest 2003;112:160–169.

9 Kocher AA, Schuster MD, Szabolcs MJ et al. Neovascularization of ischemic myocardium by human bone-marrow-derived angioblasts prevents cardiomyocyte apoptosis, reduces remodeling and improves cardiac function. Nat Med 2001;7:430–436.

10 Peled A, Petit I, Kollet O et al. Dependence of human stem cell engraftment and repopulation of NOD/SCID mice on CXCR4. Science 1999; 283:845–848.

11 Peled A, Grabovsky V, Habler L et al. The chemokine SDF-1 stimulates integrin-mediated arrest of CD34(+) cells on vascular endothelium under shear flow. J Clin Invest 1999;104:1199–1211.

12 Abe R, Shimizu T, Sugawara H et al. Regulation of human melanoma growth and metastasis by AGE-AGE receptor interactions. J Invest Dermatol 2004;122:461–467.

13 Boniface K, Bernard F-X, Garcia M et al. IL-22 inhibits epidermal differentiation and induces proinflammatory gene expression and migration of human keratinocytes. J Immunol 2005 2005;174:3695–3702.

14 Morales J, Homey B, Vicari AP et al. CTACK, a skin-associated chemokine that preferentially attracts skin-homing memory T cells. Proc Natl Acad Sci U S A 1999;96:14470–14475.

15 Homey B, Alenius H, Muller A et al. CCL27-CCR10 interactions regulate T cell-mediated skin inflammation. Nat Med 2002;8:157–165.

16 Reiss Y, Proudfoot AE, Power CA et al. CC chemokine receptor (CCR)4 and the CCR10 ligand cutaneous T cell-attracting chemokine (CTACK) in lymphocyte trafficking to inflamed skin. J Exp Med 2001;194:1541–1547.

17 Dreyfus PA, Chretien F, Chazaud B et al. Adult bone marrow-derived stem cells in muscle connective tissue and satellite cell niches. Am J Pathol 2004;164:773–779.

18 Goolsby J, Marty MC, Heletz D et al. Hematopoietic progenitors express neural genes. Proc Natl Acad Sci U S A 2003;100:14926–14931.

19 Wright DE, Bowman EP, Wagers AJ et al. Hematopoietic stem cells are uniquely selective in their migratory response to chemokines. J Exp Med 2002;195:1145–1154.

20 Tonnesen MG, Feng X, Clark RA. Angiogenesis in wound healing. J Investig Dermatol Symp Proc 2000;5:40–46.

21 Askari AT, Unzek S, Popovic ZB et al. Effect of stromal-cell-derived factor 1 on stem-cell homing and tissue regeneration in ischaemic cardiomyopathy. Lancet 2003;362:697–703.

22 Imitola J, Raddassi K, Park KI et al. Directed migration of neural stem cells to sites of CNS injury by the stromal cell-derived factor 1alpha/CXC chemokine receptor 4 pathway. Proc Natl Acad Sci U S A 2004; 101:18117–18122.

23 Yamaguchi J, Kusano KF, Masuo O et al. Stromal cell-derived factor-1 effects on ex vivo expanded endothelial progenitor cell recruitment for ischemic neovascularization. Circulation 2003;107:1322–1328.

24 Lagasse E, Connors H, Al-Dhalimy M et al. Purified hematopoietic stem cells can differentiate into hepatocytes in vivo. Nat Med 2000;6:1229.

25 Badiavas EV, Abedi M, Butmarc J et al. Participation of bone marrow derived cells in cutaneous wound healing. J Cell Physiol 2003;196:245–250.

26 Jang YY, Collector MI, Baylin SB et al. Hematopoietic stem cells convert into liver cells within days without fusion. Nat Cell Biol 2004; 6:532–539.

**CTACK/CCL27 Accelerates Skin Regeneration via Accumulation of Bone Marrow-Derived Keratinocytes**

Daisuke Inokuma, Riichiro Abe, Yasuyuki Fujita, Mikako Sasaki, Akihiko Shibaki, Hideki Nakamura, James R. McMillan, Tadamichi Shimizu and Hiroshi Shimizu

*Stem Cells* 2006;24;2810-2816; originally published online Aug 24, 2006;
DOI: 10.1634/stemcells.2006-0264

DNA REPAIR 5 (2006) 816–828

available at www.sciencedirect.com

SCIENCE DIRECT®

journal homepage: www.elsevier.com/locate/dnarepair

# Analyses of the interaction of WRNIP1 with Werner syndrome protein (WRN) *in vitro* and in the cell

*Yoh-ichi Kawabe*[a,1], *Masayuki Seki*[a,*], *Akari Yoshimura*[a], *Katsuaki Nishino*[a], *Tomoko Hayashi*[a], *Takashi Takeuchi*[a], *Sohta Iguchi*[a], *Yumiko Kusa*[a], *Makoto Ohtsuki*[a], *Takashi Tsuyama*[a], *Osamu Imamura*[b], *Takehisa Matsumoto*[c], *Yasuhiro Furuichi*[d], *Shusuke Tada*[a], *Takemi Enomoto*[a,e]

[a] *Molecular Cell Biology Laboratory, Graduate School of Pharmaceutical Sciences, Tohoku University, Aoba 6-3, Aramaki, Aoba-ku, Sendai 980-8578, Japan*

[b] *Department of Biochemistry I, National Defense Medical College, Tokorozawa 359-8513, Japan*

[c] *Protein Research Group,Genomic Sciences Center, RIKEN Yokohama Institute, Yokohama 230-0045, Japan*

[d] *Genecare Co. Ltd., 200 Kajiwara, Kamakura 247-0063, Japan*

[e] *Tohoku University 21st Century COE Program Comprehensive Research and Education Center for Planning of Drug development and Clinical Evaluation, Sendai 980-8578, Japan*

ARTICLE INFO

*Article history:*
Received 20 January 2006
Received in revised form
11 April 2006
Accepted 11 April 2006
Published on line 12 June 2006

*Keywords:*
WRN
Mgs1
WRNIP1
RecQ
FEN1
DT40
Polδ

ABSTRACT

Werner was originally identified as a protein that interacts with the product of the Werner syndrome (WS) gene, WRN. To examine the function of the WRNIP1/WRN complex in cells, we generated knock-out cell lines that were deficient in either WRN ($WRN^{-/-}$), WRNIP1 ($WRNIP1^{-/-/-}$), or both ($WRNIP1^{-/-/-}/WRN^{-/-}$), using a chicken B lymphocyte cell line, DT40. $WRNIP1^{-/-/-}/WRN^{-/-}$ DT40 cells grew at a similar rate as wild-type cells, but the rate of spontaneous sister-chromatid exchange was augmented compared to that of either of the single mutant cell lines. Moreover, while $WRNIP1^{-/-/-}$ and $WRN^{-/-}$ cells were moderately sensitive to camptothecin (CPT), double mutant cells showed a synergistic increase in CPT sensitivity. This suggested that WRNIP1 and WRN do not always function cooperatively to repair DNA lesions. The lack of a discernable functional interaction between WRNIP1 and WRN prompted us to reevaluate the nature of the physical interaction between these proteins. We found that MBP-tagged WRNIP1 interacted directly with WRN, and that the interaction was enhanced by the addition of ATP. Mutations in the Walker A motifs of the two proteins revealed that WRNIP1, but not WRN, must bind ATP before an efficient interaction can occur.



## 1. Introduction

Werner syndrome (WS) is a rare autosomal recessive disorder characterized by premature aging and the early onset of age-related diseases, including arteriosclerosis, malignant neoplasms, melituria, and cataracts [1]. Somatic cells derived from WS patients have a shorter life span in *in vitro* culture [2] and elevated rates of chromosomal translocations, rearrangements and deletions [3]. WS cells also show subtle defects in DNA replication, such as an extended S phase, and a reduced

* *Corresponding author*. Tel.: +81 22 795 6875; fax: +81 22 795 6873.
E-mail address: seki@mail.pharm.tohoku.ac.jp (M. Seki).
[1] Present address: Graduate School of Life and Environmental Sciences, University of Tsukuba, Tsukuba Science City 305-8572, Japan.

1568-7864/$ – see front matter © 2006 Elsevier B.V. All rights reserved.
doi:10.1016/j.dnarep.2006.04.006

frequency of firing of replication origins [4]. In addition, a number of reports have shown that many cellular events, including DNA repair, recombination, transcription, apoptosis, and telomere maintenance, are defective in WS cells [5].

The gene responsible for WS encodes WRN, which is a member of the RecQ family of DNA helicases [6]. WRN has been shown to possess DNA helicase and exonuclease activities [7–10]. Accumulating evidence suggests that one of the cellular role of WRN relates to telomere function, as it has been shown that WRN is necessary to prevent telomere dysfunction and subsequent genomic instability [11,12]. Additional cellular functions of WRN are not well understood, but it has been speculated that WRN is involved in many aspects of cellular metabolism, based on the identification of several WRN binding partners, including DNA polymerase δ, replication protein A (RPA), proliferating cell nuclear antigen (PCNA), flap endonuclease 1 (FEN1), DNA topoisomerase I, Ku 70/86 complex, p53, the RecQ helicase defective in Bloom syndrome (BLM), poly (ADP-ribose) polymerase, and RAD52 [5]. The functional significance of the interaction of WRN with many of these proteins is unknown, but it was reported that WRN stimulated the activity of DNA polymerase δ and FEN1 nuclease [13,14], and the Ku70/86 complex stimulated the exonuclease activity of WRN [15].

To obtain further insight into the cellular function of WRN, we previously identified several WRN-interacting proteins using the yeast two-hybrid assay, including a novel protein that we initially termed Werner helicase interacting protein (WHIP) [16]. This protein was subsequently renamed Werner interacting protein 1 (WRNIP1) in accordance with the HUGO nomenclature system. The amino acid sequence of WRNIP1 was similar to that of replication factor C (RFC) in that it contained a region of motifs, called Walker A and B, which mediate ATP binding and/or ATPase activity. In our previous study, we found that WRN and WRNIP1 co-immunoprecipitated from cellular extracts, but the function of WRNIP1 and significance of the interaction with WRN has yet to be fully elucidated. Certainly the presence of Walker A and B motifs provide important clues as to the function of WRNIP1 [16].

A homologue of *WRNIP1*, *MGS1*, has been identified in budding yeast [17]. Previous studies have shown that overproduction of Mgs1 is lethal in combination with mutations in genes that encode proteins involved in DNA replication, such as DNA polymerase δ, RFC, PCNA, and RPA [18,19]. We have previously shown that the *mgs1* mutation partially alleviated the growth defects of *pol31* mutant yeast, which bear a mutation in the second subunit of DNA polymerase δ [19]. We hypothesized that a Wrnip1 (Mgs1) interacted with the DNA replication machinery to modulate the function of DNA polymerase δ during DNA replication or replication-associated repair [19]. In support of this hypothesis, it has been reported that WRN interacts with human DNA polymerase δ through its C-terminal region [20]. It has also been shown that WRN stimulates yeast DNA polymerase δ activity *in vitro* [13], and that recombinant human WRNIP1 directly interacts with three of the four subunits of human DNA polymerase δ, and stimulated polymerase activity [21]. These observations suggest that the functions of WRN and its binding partners, including WRNIP1, are related to the regulation of DNA polymerase δ activity.

In the current study, we generated a *WRNIP1*$^{-/-/-}$/*WRN*$^{-/-}$ double-gene knockout cell line in order to examine in more detail the functional relationship between WRNIP1 and WRN. We characterized both the functional interaction of WRNIP1 and WRN using the double mutant cell line, and the physical interaction between the two proteins using purified recombinant proteins and the yeast two-hybrid assay.

## 2. Materials and methods

### 2.1. *Generation of WRNIP1*$^{-/-/-}$ *and WRNIP1*$^{-/-/-}$/*WRN*$^{-/-}$ *DT40 cells*

Cells (DT40, a chicken B lymphocyte cell line), were cultured in RPMI 1640 supplemented with 100 μg/ml kanamycin, 10% fetal bovine serum and 1% chicken serum (Sigma, St. Louis, MO, USA) at 39.5 °C. Generation of the *WRN*$^{-/-}$ knock-out cell line was reported previously [22]. Generation of the *WRNIP1*$^{-/-/-}$ DT40 cell line is detailed in the Section 3. To generate *WRNIP1*$^{-/-/-}$/*WRN*$^{-/-}$ cells, 30 μg of a linearized WRN-targeting construct were introduced into wild-type and *WRNIP1*$^{-/-/-}$ DT40 cells by electroporation using the Gene Pulser II (BioRad, Hercules, CA, USA) set at 550 V and 25 μF. Drug-resistant colonies were selected in 96-well plates in media containing 2.5 mg/ml hygromycin (Wako Pure Chemical Industries, Ltd. Japan) or 500 ng/ml puromycin. Gene disruption was confirmed by Southern blot analysis and RT-PCR. The primers used to analyze *WRNIP1*, (see Fig. 1A) *WRN*, and *RECQL1* by RT-PCR were as follows:

- *WRNIP1*-sense: 5′-CCATTCTCTTTATCGATGAGATCCATCGG-3′ [primer (a)]
- *WRNIP1*-antisense: 5′-GTTCTTCGTTCCTTGAAGAAGTCTGTTCC-3′ [primer (b)]
- *WRNIP1*-antisense: 5′-GCATTCGAGCAAGCCAGTAGAG-3′ [primer (c)]
- *WRN*-sense: 5′-CAGTGGAAAGTGATACATTCTGTTTTAGAAGAC-3′
- *WRN*-antisense: 5′-CACCTGCAATTATCACAGCACTATTC-3′
- *RECQL1*-sense: 5′-ATGACAGCTGTGGAAGTGCTAGAGGA-3′
- *RECQL1*-antisense: 5′-TCAGTCAAGAACAACAGGTTGGTCATCTC-3′

### 2.2. *Southern blot analysis*

Thirty micrograms of genomic DNA isolated from wild-type and/or the various DT40 mutant cell lines were digested by *BamHI*, then separated by agarose gel electrophoresis. DNA was transferred to Hybond-N filters (Amersham Pharmacia), then subjected to hybridization at 42 °C overnight in 5 × SSPE buffer containing 50% formamide, 2% SDS, 10× Denhardt's solution, and 100 μg/ml denatured salmon sperm DNA, using an [α-$^{32}$P]dCTP-labeled chicken *WRNIP1* cDNA as a probe. The filter was then washed as follows: three washes with 2× SSC – 0.1% SDS for 15 min at room temperature followed by one wash with 1× SSC – 0.1% SDS for 15 min at 42 °C. The hybridized DNA fragments were visualized by autoradiography.

### 2.3. *Growth curves and flow cytometry*

Cells (5 × 10$^4$) were cultured at 39.5 °C for varying periods of time, after which they were counted to determine their growth rate. To determine the cell cycle distribution, cells were filtered through a nylon mesh, then analyzed using a FACScan (Becton Dickinson, Mountain View, CA). The FACS data were processed using Cell Quest software (Becton Dickinson).

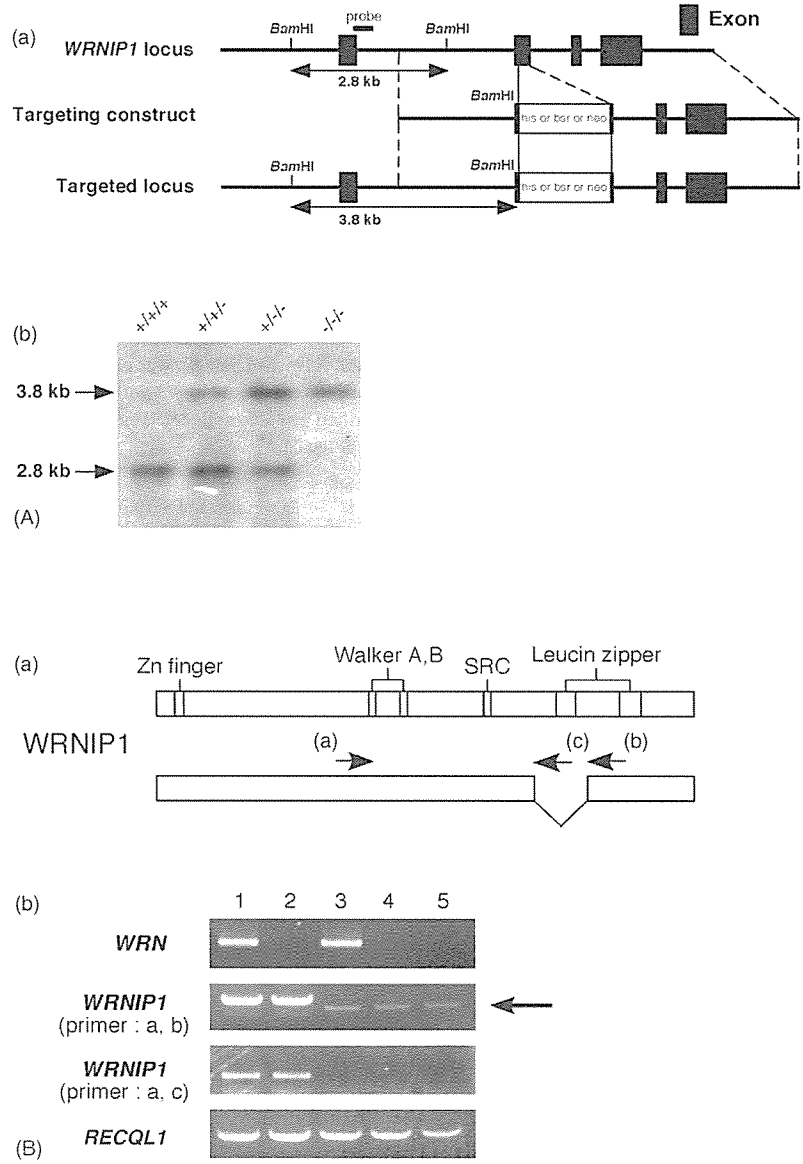


**Fig. 1 – Generation of *WRNIP1*$^{-/-/-}$ and *WRNIP1*$^{-/-/-}$/*WRN*$^{-/-}$ DT40 cells. (A) Panel a: schematic representation of the chicken *WRNIP1* genomic locus, the targeting constructs used in these studies, and the genomic arrangement of the targeted locus. Panel b: to confirm the status of the *WRNIP1* locus of wild-type (+/+/+), heterozygous (+/+/− and +/−/−), and homozygous (−/−/−) null cells, the *Bam*HI-digested genomic DNA was examined by Southern blot analysis using a probe corresponding to the region indicated in panel a. (B) Panel a: schematic representation of the wild-type WRNIP1, and the WRNIP1 deletion mutant expressed in *WRNIP1*$^{-/-/-}$ and *WRNIP1*$^{-/-/-}$/*WRN*$^{-/-}$ cells. The primers used to amplify *WRNIP1* transcripts are also indicated (a, b and c). Panel b: RT-PCR analysis of total RNA from wild-type (lane 1), *WRN*$^{-/-}$ (lane 2), *WRNIP1*$^{-/-/-}$ (lane 3), and *WRNIP1*$^{-/-/-}$/*WRN*$^{-/-}$ cells (lanes 4 and 5). Primers a and b were used to detect both full length and the deletion mutant (arrow) of *WRNIP1*, while primers a and c were used to detect full length mRNA transcripts. The primers used to detect *WRN* and *RECQL1* mRNA are described in Section 2.**

### 2.4. *Measurement of drug sensitivity*

A stock solution of 10 mM CPT (Sigma) in DMSO was stored at −20 °C. Individual aliquots were removed and diluted into cell culture medium immediately prior to each experiment. An amount of 2–6 × $10^2$ cells were inoculated into medium supplemented with 1.5% (w/v) methylcellulose, 1.5% chicken serum and 15% fetal bovine serum containing various concentrations of methylmethane sulfonate (MMS), cisplatin (CDDP), 4-nitroquinoline-1-oxide (4-NQO), or CPT. After 10 days, visible colonies were counted. The data represent the percent survival compared to untreated cells.

### 2.5. *Measurements of spontaneous sister chromatid exchange (SCE)*

Cells (5 × $10^5$) were cultured for two cell cycles in medium containing 10 μM BrdU, then treated with 0.1 μg/ml colcemid for 2.5 h. Cells were

harvested, incubated in 75 mM KCl for 12 min at room temperature, and then fixed by suspension in methanol–acetic acid (3:1) for 30 min. The cell suspension was dropped onto ice-cold wet glass slides and air-dried, then the slides were incubated with 10 μg/ml Hoechst 33258 in phosphate buffer (pH 6.8) for 20 min, followed by washing with McIlvaine solution (164 mM $Na_2HPO_4$, 16 mM citric acid, pH 7.0). The glass slides were then exposed to black light (λ = 352 nm) at a distance of 1 cm for 20 min followed by incubation in 2× SSC (0.3 M NaCl, 0.03 M sodium citrate) at 58 °C for 20 min. Finally, the cells on the slides were stained with 3% Giemsa solution for 25 min.

### 2.6. Yeast strains

The following yeast strains used in this study have been described previously [19,23]: *KSH542 MATa ade1 his2 his3-200 trp1 ura3 leu2 hys2-1; PY82 MAT ade2-101 leu2-3, 112 lys2-801 ura3-52 his3-200 pol32::HIS3; MR101 MATa/α ura3-52/ura3-52 leu2-3,112/leu2-3,112 trp1-289/trp1-289 his1-7/his1-1; MRdw MATa/α ura3-52/ura3-52 leu2-3,112 leu2-3,112 trp1-289/trp1-289 his1-7/his1-1 mgs1::KANMX4/mgs1::KANMX4.*

### 2.7. Spot assay

*hys2-1* (KSH542) and *pol32Δ* yeast carrying plasmid DNA encoding wild-type Mgs1 or Mgs1 Δ399–445, or an empty expression vector (pYES2) as a control, were grown in raffinose SC-Ura medium, diluted, and spotted onto SC-Ura plates containing glucose or galactose.

### 2.8. Measurement of spontaneous heteroallelic recombination

The frequency of interchromosomal recombination in diploid cells between the heteroalleles *his1-7* and *his1-1* was measured in wild-type (MR101) and *mgs1* mutant (MRdw) yeast carrying DNA encoding wild-type MGS1, MGS1 Δ399–445, or the empty expression vector (YCplac122) as a control. Yeast cells were spread onto SD-Trp or SD-Trp-His plates, and the plates were incubated at 30 °C for 3 days, after which the number of colonies was counted. Recombination frequency was calculated as the number of $His^+$ colonies per $10^6$ viable cells.

### 2.9. Generation of a WRN baculovirus expression system

A cDNA encoding full-length mouse WRN (mWRN) was amplified from a plasmid harboring a full-length *mWRN* cDNA [24] by PCR using Pfu DNA polymerase (Stratagene). The amplified product was then digested with *XbaI* and *XhoI* and subcloned into the *XbaI* and *XhoI* sites of pFastBac HT, a transfer vector of the Bac-To-Bac Baculovirus expression system (Gibco-BRL). The insertion site of the *mWRN* cDNA was downstream of the hexa-histidine sequence and was preceded by the baculovirus polyhedron promoter. The expression cassette containing wild-type *mWRN* was transferred to bacmid DNA by transfecting the vectors into DH10Bac competent cells. PCR confirmed that the Tn7 transposition specific reaction had successfully transferred *mWRN* into bacmid DNA. Sf21 cells were transfected with *mWRN* bacmid DNA and recombinant viruses were recovered 4–5 days after the infection.

### 2.10. Expression and purification of recombinant mWRN

Sf9 cells infected with recombinant virus encoding *mWRN* were incubated for 2 days and then collected by centrifugation. The cells were washed with cold calcium- and magnesium-free phosphate-buffered saline (PBS) and stored at −80 °C until use. To purify WRN, cells were thawed, suspended in hypotonic buffer (10 mM HEPES–NaOH, pH 7.9, 0.5% Nonidet P-40, 1 mM $MgCl_2$, 0.5 mM $CaCl_2$, 1 mM benzamidine, 0.2 mM phenylmethylsulfonyl fluoride (PMSF)) and incubated on ice for 10 min. The nuclei were then collected, resuspended in lysis buffer (15 mM HEPES–NaOH, pH 7.9, 5 mM $MgCl_2$, 400 mM NaCl, 1 mM benzamidine, 0.2 mM PMSF), and incubated on ice for 30 min. After clarification by centrifugation, the nuclear extracts were incubated with $Ni^{2+}$-charged chelating Sepharose (Amersham Pharmacia) at 4 °C for 1 h. The resin was then washed with 50 mM HEPES–NaOH, pH 7.9, 1 mM $MgCl_2$, 10% glycerol, 100 mM imidazole, 1 mM benzamidine, 0.2 mM PMSF containing 300 mM NaCl, and then washed a second time in the same buffer with 100 mM NaCl. The proteins that remained bound to the resin were eluted in a solution of 20 mM Tris–HCl, pH 7.5, 1 mM $MgCl_2$, 100 mM NaCl, 10% glycerol, 500 mM imidazole, 1 mM benzamidine, and 0.2 mM PMSF. Eluted fractions were applied to a HiTrap Heparin column (Amersham Pharmacia) and washed with WS buffer (20 mM Tris–HCl, pH 7.5, 1 mM 2-mercaptoethanol, 1 mM $MgCl_2$, 10% glycerol, 1 mM benzamidine, and 0.2 mM PMSF) containing 100 mM NaCl. Adsorbed protein was eluted in a linear gradient of NaCl ranging from 100 to 900 mM in WS buffer. The purity of the eluted fractions was verified by sodium dodecyl sulfate-polyacrylamide gel electrophoresis (SDS-PAGE).

### 2.11. Expression and purification of recombinant maltose-binding protein (MBP)-tagged mouse WRNIP1

*E. coli* BL21 (DE3) cells were transduced with an expression vector encoding MBP-mWRNIP1 (pMAL-mWRNIP1) [16], and grown at 37 °C to an optical density of 0.4–0.7 at 600 nm. Isopropyl-β-D-thiogalactopyranoside (0.1 mM) was added to the culture to induce expression of the recombinant protein, and the cells were incubated for an additional 3 h. Cells were then collected by centrifugation, washed with cold PBS and stored at −80 °C until use. Cells were thawed and resuspended in MS buffer (20 mM Tris–HCl, pH 7.5, 1 mM dithiothreitol, 10% glycerol, 1 mM benzamidine, 0.2 mM PMSF) containing 1% Triton X-100, 100 mM NaCl, and 0.1 mM EDTA, then disrupted by sonication. The cell lysate was clarified by centrifugation and incubated with amylose resin (New Englands Biolabs) for 1 h at 4 °C. The resin was washed with MS buffer containing 500 mM NaCl, then washed a second time in MS buffer containing 100 mM NaCl. Proteins were eluted with MS buffer containing 100 mM NaCl and 30 mM maltose, applied to a Q Sepharose (Amersham Pharmacia) column, washed with 100 mM NaCl in MS buffer and then eluted in a linear gradient of NaCl ranging from 100 to 500 mM in MS buffer. As a control, MBP was purified from BL21 (DE3) cells transfected with the pMAL-c2 vector using the same procedure. The purity of the eluted fractions was verified by SDS-PAGE.

### 2.12. In vitro interaction assay

Purified mWRN (15 μg) and 20 μl of amylose resin bearing either MBP-mWRNIP1 or MBP were incubated in 300 μl of IR buffer (50 mM Tris–HCl, pH 7.5, 1 mM 2-mercaptoethanol, 4 mM $MgCl_2$, 5 mM ATP, 1 mM benzamidine, 0.2 mM PMSF) for 3 h at 4 °C, then the resin was collected by centrifugation. The supernatant, representing the unbound fraction, was also collected. The resin was washed twice with 150 μl of IR buffer, and adsorbed proteins were eluted with 30 μl of IR buffer containing 30 mM maltose. Proteins in the supernatant and in the eluted fractions were analyzed by SDS-PAGE and visualized by silver staining.

### 2.13. Co-expression of FLAG-WRNIP1, HA-WRNIP1, immunoprecipitation, and immunoblotting

Human 293EBNA cells were cultured in Dulbecco's modified Eagle's medium supplemented with 10% fetal bovine serum, grown to 70% confluence in 10-cm dishes, then transfected with plasmid DNA using LipofectAMINE (Life Technologies, Inc.). The culture medium was changed 24 h later and the cells were incubated for an additional 24 h. Cells were washed once with PBS, then lysed in 0.5% Triton buffer (50 mM Tris–HCl, pH 7.6, 150 mM NaCl, 0.5% Triton X-100, 1 mM dithiothreitol) containing COMPLETE protease inhibitor cocktail (Roche Molecular Biochemicals)

on ice for 20 min. Lysates were subjected to immunoprecipitation and immunoblotting as described previously [16].

### 2.14. *Two-hybrid assays*

The yeast strains and plasmids used in the two-hybrid assays have been described previously [24]. The yeast two-hybrid assay was carried out according to the manufacturers instructions (CLONTECH). Plasmids encoding mWRNIP1, mWRN, and the various point mutants of each were generated as follows: point mutations were generated by PCR-based site-directed mutagenesis; deletion mutations were generated by PCR, then subcloned into the pGAD vector. The details of the methods used to generate the mutants, including primer sequences, will be provided upon request.

## 3. Results

### 3.1. *Generation of DT40 WRNIP1$^{-/-/-}$ mutant cell lines*

To examine the cellular function of WRNIP1, we generated *WRNIP1* gene knockout cells using the chicken DT40 cell line. A partial cDNA encoding the C-terminal region of chicken *WRNIP1* (Accession No. AB104724) was amplified by reverse transcription-polymerase chain reaction (RT-PCR) using total RNA purified from DT40 cells as the template. Full-length chicken *WRNIP1* (Accession No. XM_418979) showed 63.0%, 63.9%, 55.9% and 23.9% identity to its human, mouse, frog (Accession No. AB212951), and budding yeast counterparts, respectively (Supplementary Figure 1).

The DNA sequence of the partial cDNA of *WRNIP1* was confirmed, and we used this fragment as a probe to isolate a *WRNIP1* genomic DNA fragment of about 5.5 kb. This genomic fragment contained the exons encoding the C-terminal region of WRNIP1, and was used to generate the *WRNIP1* targeting constructs, *WRNIP1-his*, *WRNIP1-bsr*, and *WRNIP1-neo* (Fig. 1A, panel a). The three different selection markers were each inserted into the targeting vector *via* a *Bam*H1 site that was generated using site-directed mutagenesis. The marker insertion site was located in a highly conserved Leucine zipper domain in vertebrate WRNIP1 (Supplementary Figure 1). Gene disruption was confirmed by the appearance of a 3.8 kb genomic fragment in Southern blot hybridization experiments using an internal *WRNIP1*-specific probe (Fig. 1A, panels a and b). There are three alleles of *WRNIP1* in DT40 cells, due to triplication of chromosome 2. We disrupted the third allele using the *WRNIP1-neo* targeting construct, and confirmed this disruption by Southern blot analysis (Fig. 1A, panel b). As shown in Fig. 1B, panel b, a faint 874 bp fragment was observed after RT-PCR analysis of total RNA purified from *WRNIP1*$^{-/-/-}$cells, using primers (a) and (b) (Fig. 1B, panel a). In contrast, a 1030 bp fragment was amplified from wild-type cells using the same set of primers. Sequence analysis of the 874 bp fragment revealed that it encoded a deletion mutant of WRNIP1 lacking 52 amino acids (amino acids 393–444). This suggested that the *WRNIP1* mRNA transcript of the disrupted gene in *WRNIP1*$^{-/-/-}$ DT40 cells was subject to illegitimate splicing. When primers (a) and (c) were used for RT-PCR analysis, we amplified a product only from wild-type cells, and not *WRNIP1*$^{-/-/-}$ cells. Taken together, these observations indicated that a low level of a deletion mutant of WRNIP1 was expressed in *WRNIP1*$^{-/-/-}$ cells.

### 3.2. *Truncated yWRNIP1 (MGS1) is a functional null mutant*

We were interested in whether the truncated form of WRNIP1 that appeared to be expressed *WRNIP1*$^{-/-/-}$ DT40 cells retained significant biological activity. To examine this, we took advantage of an earlier observation that overproduction of wild-type *S. cerevisiae* yWrnip1 (Mgs1) is lethal in yeast that carry mutations in the small subunits of DNA polymerase δ, namely, *hys2-1* (pol31) and *pol32Δ* [19]. We constructed an *MGS1* deletion mutant in which the deleted region corresponded to the deleted region of WRNIP1 in *WRNIP1*$^{-/-/-}$ DT40 cells (Fig. 2A and Supplementary Figure 1), and examined the effect of overexpression of this gene in *hys2-1* and *pol32Δ*yeast. Overexpression of this mutant of Mgs1 was not lethal in *hys2-1* or *pol32* Δyeast (Fig. 2B and C). In a separate assay (Fig. 2D, panel a), introduction of wild-type *MGS1* suppressed the elevated frequency of spontaneously occurring interchromosomal recombination in *mgs1* diploid *S. cerevisiae* [23], while the *MGS1* deletion mutant failed to substantially suppress this phenotype (Fig. 2D, panel b). These results indicated that the deletion mutant of yWrnip1 (Mgs1) is a functional null mutant.

### 3.3. *Generation of WRN$^{-/-}$ and WRNIP1$^{-/-/-}$/WRN$^{-/-}$ mutant cells*

To determine the functional relationship between WRN and WRNIP1 in vertebrate cells, we generated a single mutant cell line, *WRN*$^{-/-}$ DT40, and a double mutant cell line, *WRNIP1*$^{-/-/-}$*/WRN*$^{-/-}$ DT40. To do this, two WRN-targeting constructs [22] were transfected sequentially into wild-type or *WRNIP1*$^{-/-/-}$ cells. *WRN* gene disruption was verified by Southern blot analysis (data not shown), as described previously [22], and by RT-PCR (Fig. 1B, panel b). These results showed that a double gene knock-out cell line, *WRNIP1*$^{-/-/-}$*/WRN*$^{-/-}$, was successfully established.

### 3.4. *Proliferation of WRNIP1$^{-/-/-}$/WRN$^{-/-}$ DT40 cells*

The *mgs1/sgs1* budding yeast double mutant (*mgs1/sgs1* are the counterparts of vertebrate *WRNIP1/WRN*) exhibited a severe growth defect compared to either of the corresponding yeast single mutants [17,23]. Thus, we were interested in whether *WRNIP1* gene disruption affected the growth rate of *WRN*$^{-/-}$ cells. *WRNIP1*$^{-/-/-}$*/WRN*$^{-/-}$ DT40, like *WRNIP1*$^{-/-/-}$ and *WRN*$^{-/-}$ DT40 cells, had a similar rate of growth to that of wild-type cells (Fig. 3A). In addition, analysis of the cells using flow cytometry indicated that the cell cycle distribution of both the single and double knockout cells was similar to wild-type cells (data not shown).

### 3.5. *Sister chromatid exchange in WRNIP1$^{-/-/-}$/WRN$^{-/-}$ cells*

Sister chromatid exchange (SCE) is an extremely sensitive marker of defects in DNA replication. As shown in Fig. 3B, there was a slight increase in spontaneous SCE in *WRNIP1*$^{-/-/-}$

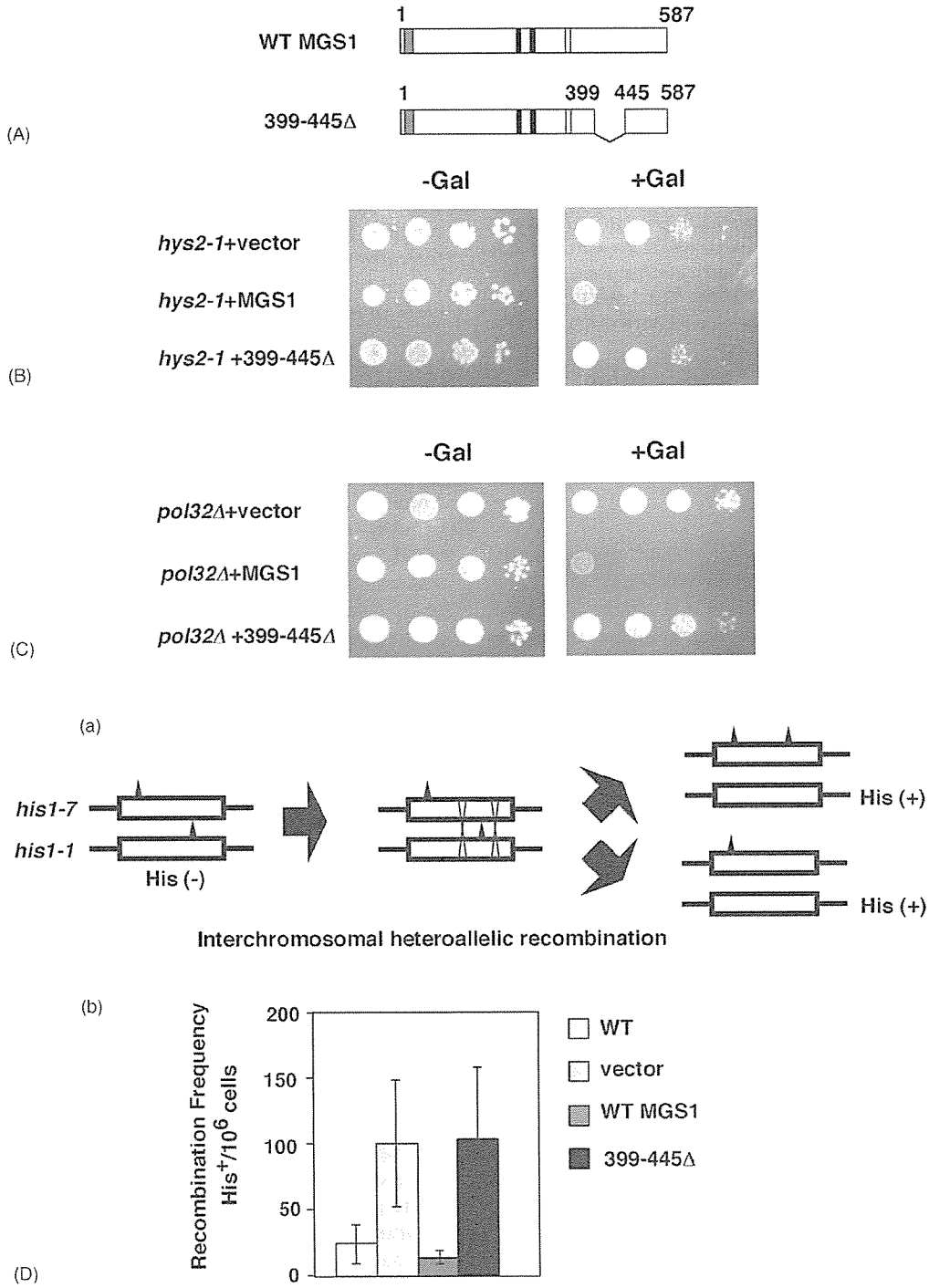


Fig. 2 – Functional analysis of the deletion mutant of yWRNIP1 (Mgs1) in budding yeast. (A) Schematic representation of the wild-type or truncated Mgs1 protein used in this study. (B) Overexpression of Mgs1 in *hys2-1* (*pol31*) yeast. Strain KSH552 yeast carrying the empty expression vector (pYES2), expressing wild-type Mgs1 or the deletion mutant Mgs1 399–445Δ were grown in raffinose SC-Ura medium, diluted, and spotted onto SC-Ura plates containing glucose or galactose. (C) Overexpression of *MGS1* in *pol32Δ* mutant yeast. Strain PY82 (*pol32Δ*) yeast containing an empty expression vector (pYES2), or the same plasmid encoding wild-type Mgs1 or the deletion mutant Mgs1 399–444*Δ*, were grown in raffinose SC-Ura medium, diluted, and spotted onto SC-Ura plates containing glucose or galactose. (D) Panel a: schematic representation of interchromosomal recombination between the heteroalleles *his1-7* and *his1-1* in diploid cells. Panel b: the frequency of heteroallelic recombination in wild-type (MR101) and *mgs1* yeast (MRdw) containing empty expression vector (YCplac122), or the same vector encoding the indicated MGS1 constructs. Wild-type and mutant yeast were spread onto SD-Trp or SD-Trp-His plates. The plates were incubated at 30 °C for 3 days, after which the colonies were counted and the recombination frequencies were calculated. Data represents the number of $His^+$ colonies per $10^6$ viable cells.

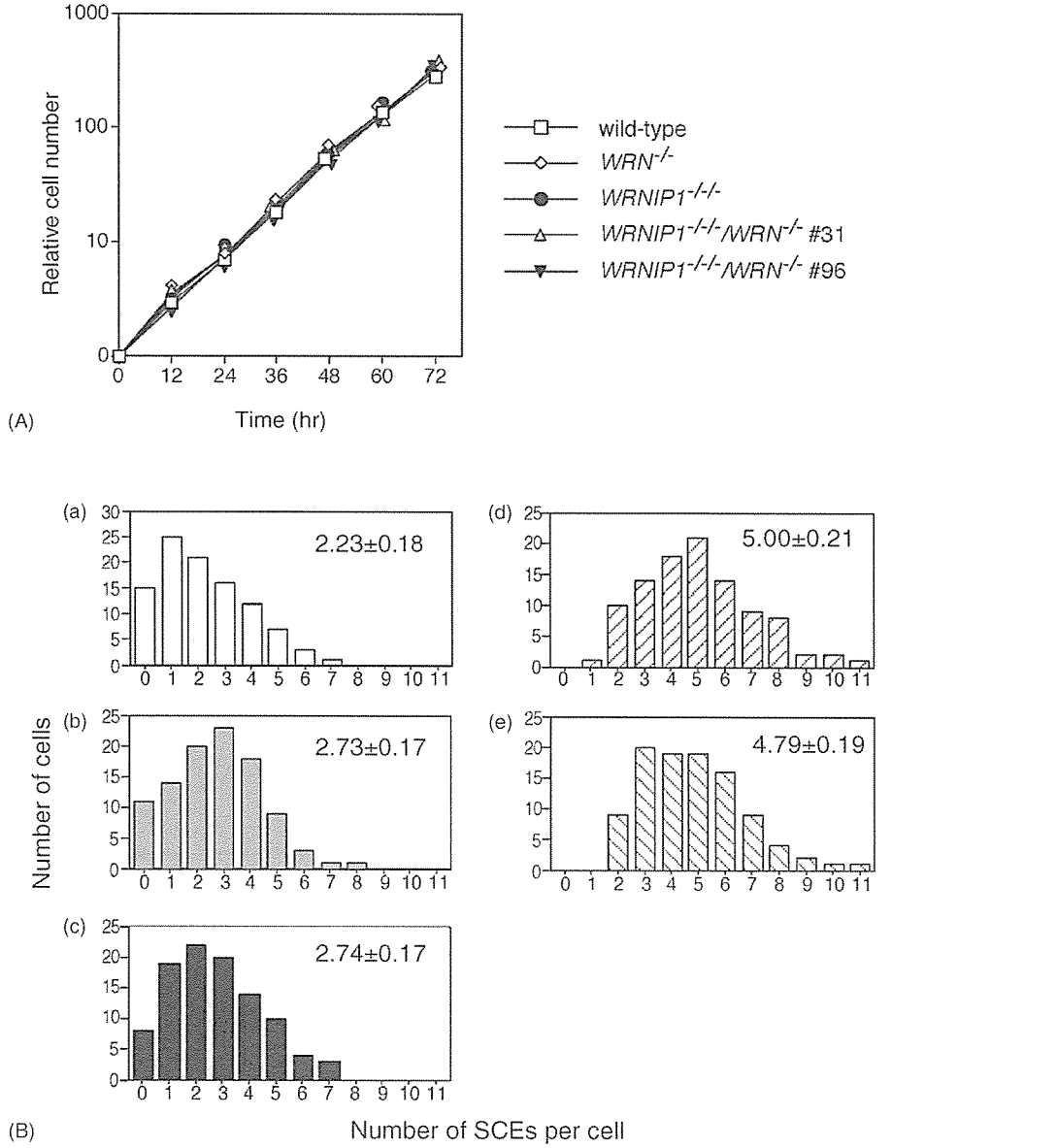


**Fig. 3 – Growth and frequency of SCE in *WRNIP1*$^{-/-/-}$/*WRN*$^{-/-}$ cells. (A) Growth curves of wild-type, *WRN*$^{-/-}$, *WRNIP1*$^{-/-/-}$, and *WRNIP1*$^{-/-/-}$/*WRN*$^{-/-}$ DT40 cells. Cells were inoculated into 60-mm dishes and counted after the indicated periods. Cells that were negative for trypan blue staining were counted as viable cells. (B) Histograms of the incidence of SCE in wild-type (a), *WRN*$^{-/-}$ (b), *WRNIP1*$^{-/-/-}$ (c), and two independently derived *WRNIP1*$^{-/-/-}$/*WRN*$^{-/-}$ cell lines (d and e). The number of spontaneous SCE events in the macro-chromosomes of 100 metaphase cells were counted. The histograms show the frequencies of cells with the indicated number of SCEs per cell. The mean and standard error of the number of SCEs per cell are shown in the upper right corner of each histogram.**

and *WRN*$^{-/-}$ cells as compared to wild-type cells, and there was an additive effect on the frequency of SCE in the *WRNIP1*$^{-/-/-}$/*WRN*$^{-/-}$ double mutant (Fig. 3B). These results indicated that WRNIP1 suppresses SCE independently of WRN.

### 3.6. *Elevated CPT sensitivity in WRNIP1*$^{-/-/-}$/*WRN*$^{-/-}$ *double mutant cells*

*WRN*$^{-/-}$ DT40 cells were moderately sensitive to MMS, CDDP, 4-NQO, and CPT compared to wild-type cells (Fig. 4), in agreement with what has been previously reported [22]. In contrast, the sensitivity of *WRNIP1*$^{-/-/-}$ cells to MMS, CDDP, and 4-NQO was similar to that of wild-type cells, and there was little to no enhancement of sensitivity in *WRNIP1*$^{-/-/-}$/*WRN*$^{-/-}$ cells over that seen in the single *WRN*$^{-/-}$ mutant cell line (Fig. 4A–C). This data suggested that WRNIP1 is not a functional component of WRN-dependent DNA repair pathways in response to lesions generated by MMS, CDDP, or 4NQO. *WRNIP1*$^{-/-/-}$ cells were moderately sensitive to CPT, to a degree comparable to that seen in *WRN*$^{-/-}$ cells, and there was a synergistic

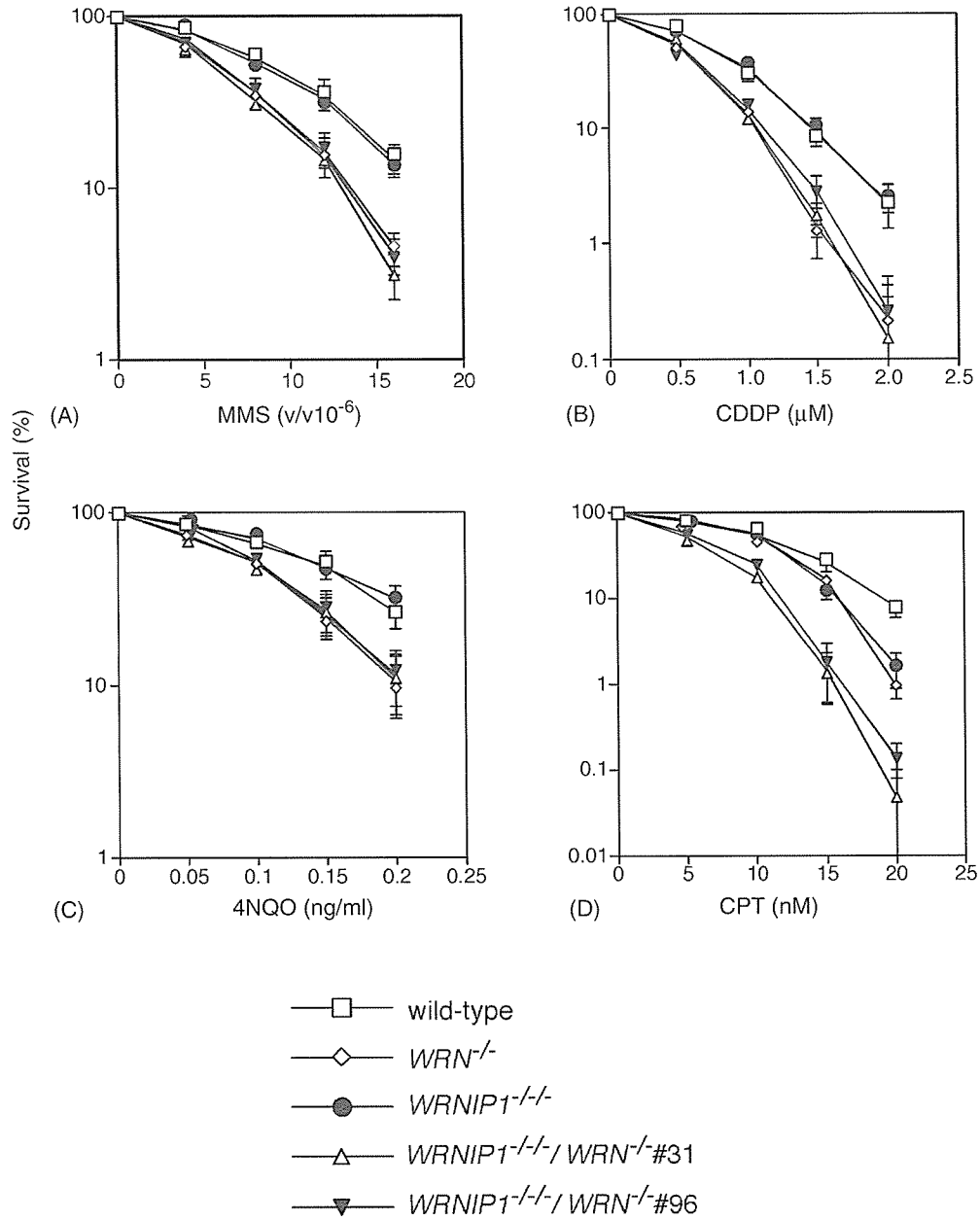


**Fig. 4 – Sensitivity of WRN$^{-/-}$, WRNIP1$^{-/-/-}$ or WRNIP1$^{-/-/-}$/WRN$^{-/-}$ DT40 cells to MMS, CDDP, 4NQO and CPT. The indicated cells were treated with the indicated concentrations of MMS (A), CDDP (B), 4NQO (C), or CPT (D) as described in Section 2. Percent survival represents the number of colonies in the presence of the indicated chemical, compared to the number of colonies in the absence of genotoxin. Symbols and lines represent the means and standard deviations calculated based on the data from three independent experiments.**

increase in sensitivity to CPT in the WRNIP1$^{-/-/-}$/WRN$^{-/-}$ double mutant cell line (Fig. 4D).

### 3.7. *Purification of recombinant mouse WRN and WRNIP1*

We previously showed that when mouse WRN fused to the FLAG epitope (FLAG-mWRN) and mouse WRNIP1 fused to a hemagglutinin (HA) epitope (HA-mWRNIP1) were ectopically expressed in human 293EBNA cells, WRNIP1 was present in anti-FLAG immune complexes isolated from these cells. [16]. We also showed that mWRN obtained by *in vitro* translation in rabbit reticulocyte lysates interacted with mWRNIP1 fused to maltose-binding protein (MBP-mWRNIP1) [16]. These observations suggested that WRNIP1 directly interacted with WRN. Since there was little evidence to support a functional relationship between WRNIP1 and WRN from our analyses of the single and double gene knockout DT40 cells, we reevaluated the physical interaction of WRNIP1 and WRN. First, to eliminate the possibility that WRNIP1 interacted with WRN indi-

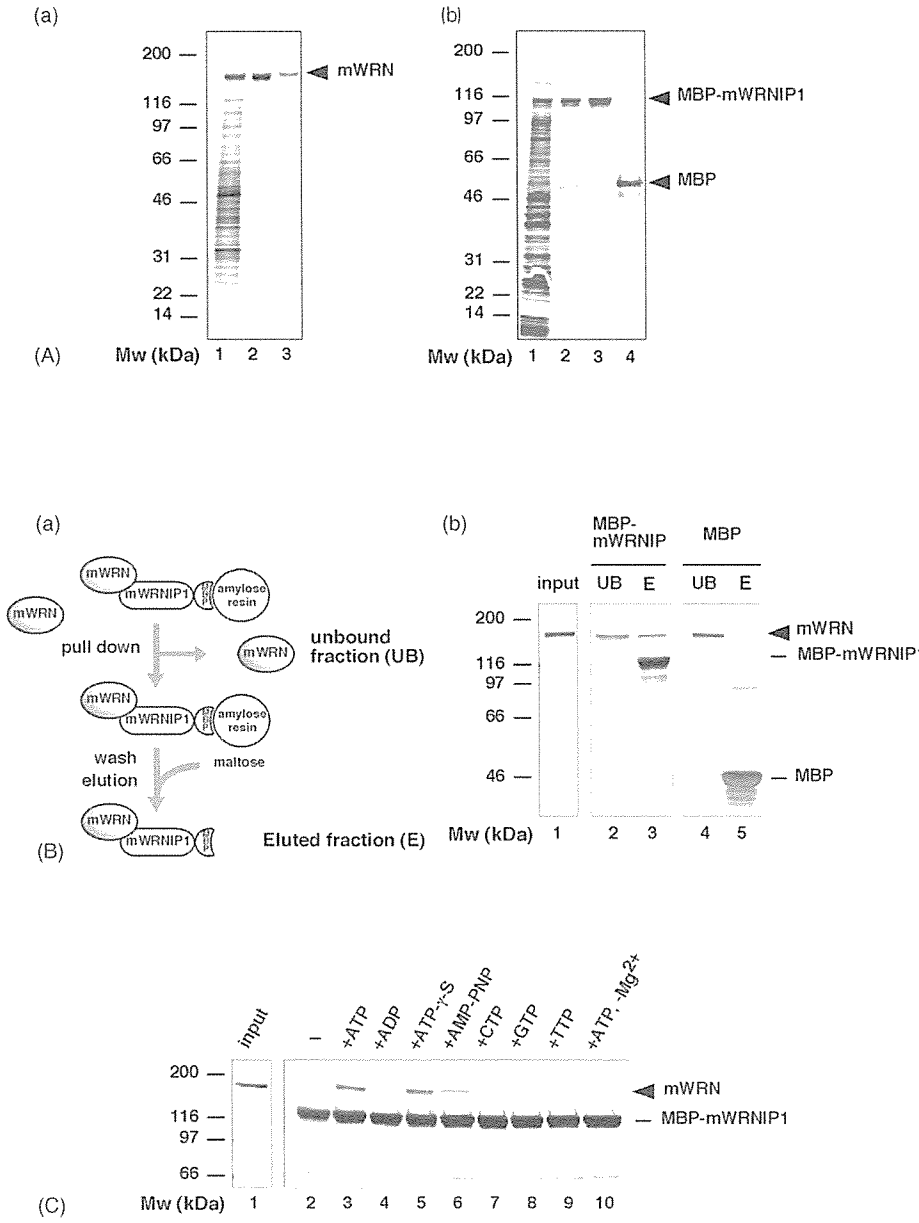


Fig. 5 – ATP stimulates the binding of WRNIP1 to WRN. (A) Purification of recombinant mWRN and mWRNIP1. Panel a: mWRN was expressed in Sf9 cells and purified as described in Section 2. A sample of whole cell lysates of Sf9 cells expressing mWRN (lane 1) and the Ni-chelating Sepharose fraction of mWRN (lane 2), and the heparin column fraction of mWRN (lane 3) were analyzed by SDS-PAGE (4–20% gradient gel) and visualized by silver staining. Panel b: MBP-mWRNIP1 was expressed in *E. coli* and purified as described in Section 2. Samples taken at each step of the purification process were subjected to SDS-PAGE (4–20% gradient gel) and visualized by silver staining. Lane 1, lysate of *E. coli* cells expressing MBP-mWRNIP1; lane 2, the amylose resin fraction of MBP-WRNIP1; lane 3, the Q-Sepharose fraction of MBP-WRNIP1; lane 4: purified MBP. (B) Physical interaction between mWRN and mWRNIP1. Panel a: schematic representation of the *in vitro* binding assay, as described in Section 2. Panel b: purified mWRN (15 μg) was incubated with 20 μl of amylose resin bearing MBP-mWRNIP1 or MBP in 300 μl of IR buffer. The reaction mixture was centrifuged and the supernatant was collected for measuring the unbound fraction of mWRN (UB). The resin was then washed and the proteins were eluted with IR buffer containing maltose (E). The UB and E fractions were analyzed by SDS-PAGE and visualized by silver staining. (C) The physical interaction between mWRN and mWRNIP1 requires nucleotides and magnesium. Purified mWRN (15 μg) was incubated with 20 μl of amylose resin bearing MBP-mWRNIP1 in 300 μl IR buffer containing 5 mM of the indicated nucleotides. Eluted fractions were analyzed by SDS-PAGE and visualized by silver staining. –, no nucleotide; $-Mg^{2+}$, no magnesium ion.

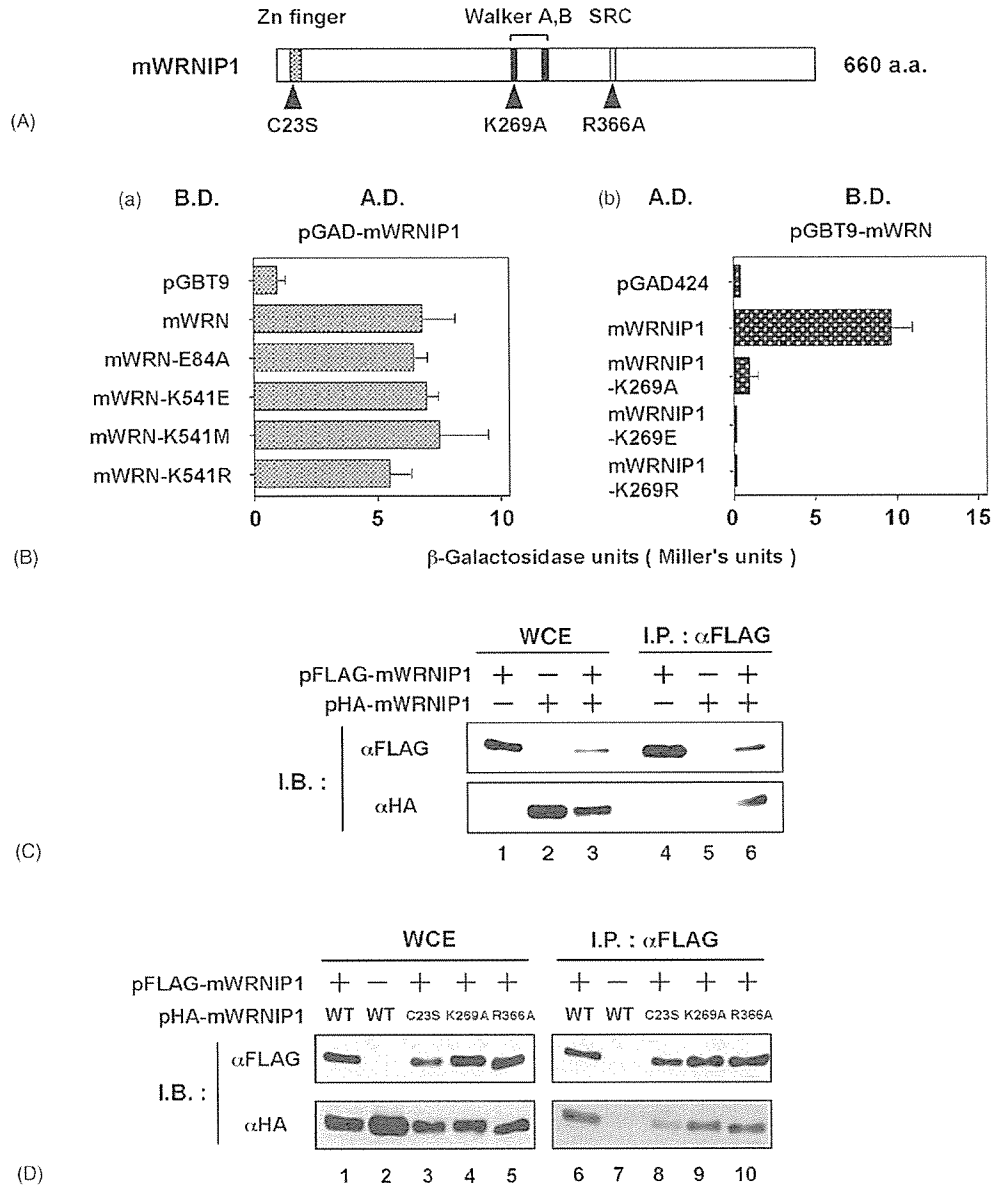


Fig. 6 – The Walker A motif of WRNIP1 is important for the interaction between WRNIP1 and WRN. (A) Schematic representation of the WRNIP1, indicating locations of the various functional domains and the various mutant constructs used in this study. (B) Effect of a mutation in the Walker A domain on the association between WRN and WRNIP1 in the yeast two-hybrid assay. Panel a: pGBT9 carrying encoding wild type, the exonuclease mutant (E84A), or indicated Walker A mutants (K541) of mWRN was co-transfected with pGAD-mWRNIP1, or a control plasmid, into yeast strain Y190. β-galactosidase activity was assayed as described previously [16]. Panel b: pGAD424 encoding wild type or the indicated Walker A mutants of mWRNIP1 was co-transfected with pGBT9-mWRN, or a control plasmid, into yeast strain Y190, and β-galactosidase activity was assayed. (C) Co-immunoprecipitation of WRNIP1. 293EBNA cells transfected with pFLAG-mWRNIP1 and pHA-mWRNIP1 were harvested, lysed, and FLAG-mWRNIP1 was immunoprecipitated using an anti-FLAG antibody. Whole cell extracts (WCEs) and the immunoprecipitates (I.P.: αFLAG) were subjected to SDS-PAGE using 7% polyacrylamide gels. Ectopically expressed mWRNIP1 was visualized by western blotting using anti-FLAG and anti-HA antibodies. The minus symbol indicates the transfection of pFLAG or pHA instead of pFLAG-mWRNIP1 or pHA-mWRNIP1, respectively. (D) Effect of the indicated mutations on self-association of WRNIP1. 293EBNA cells were co-transfected with pFLAG-mWRNIP1 and pHA encoding the indicated mutants of mWRNIP1. Forty-eight hours post-transfection, the cells were lysed and FLAG-mWRNIP1 was immunoprecipitated using an anti-FLAG antibody. Whole cell extracts (WCEs) and the immunoprecipitates (I.P.: αFLAG) were subjected to SDS-PAGE using 7% polyacrylamide gels. Self-association of mWRNIP1 was detected by western blotting using anti-FLAG and anti-HA antibodies. (–) Transfection with the control plasmid. C23A, K269A, and R266A indicate amino acid substitutions in the Zn finger domain, the Walker A motif, and the SRC domain of mWRNIP1, respectively.

rectly, *via* an adaptor or bridging protein(s) present in 293EBNA cells or rabbit reticulocyte lysate, full-length mWRN fused to a hexahistidine-tag (His-mWRN) was expressed in insect cells using a baculovirus expression system and purified using Ni-charged chelating-Sepharose and HiTrap Heparin columns. We also purified MBP-mWRNIP1 as described previously [16]. SDS-PAGE analysis demonstrated these purified preparations of His-mWRN and MBP-mWRNIP1 contained a single major band of about 160 or 120 kD, respectively (Fig. 5A).

### 3.8. *The binding of mWRNIP1 to mWRN is potentiated by ATP*

To examine whether mWRNIP1 interacted directly with mWRN, MBP-mWRNIP1 bound to an amylose resin was incubated with purified His-mWRN in the presence of ATP and magnesium. After thorough washing, proteins that remained bound to the resin were eluted with maltose (Fig. 5B, panel a). As shown in Fig. 5B, panel b, His-mWRN was eluted from MBP-mWRNIP1-bearing amylose resin (lane 3), but not from resin that was bound to MBP alone (lane 5). This indicated that MBP-mWRNIP1 bound directly to His-mWRN. When ATP was omitted form the incubation solution, the association of mWRNIP1 and mWRN was markedly reduced (Fig. 5C, lane 2). We then examined the effect of various nucleotides on the interaction between WRN and WRNIP1. As shown in Fig. 5C, addition of ADP, CTP, GTP, and TTP had no effect on binding (lanes 4, 7, 8, and 9), whereas the non-hydrolyzable ATP analogs ATP-γ-S and AMP-PNP (lanes 5 and 6) enhanced the binding of mWRNIP1 to mWRN, to the level of that observed in the presence of ATP. Omitting magnesium from the incubation medium also reduced the binding of mWRNIP1 and mWRN (lane 10). Thus, it appeared that the ATP-$Mg^{2+}$ complex enhanced the affinity between mWRNIP1 and mWRN.

### 3.9. *The Walker A motif of WRNIP1 is required for its interaction with WRN but not for self-association*

Walker A and B motifs are hallmarks of ATP-binding and/or ATPase activity. Since both WRN and WRNIP1 have these motifs (Fig. 6A), we were interested in whether a mutation of the Walker A motif of WRN or WRNIP1 affected the interaction between the two proteins. Using a yeast two-hybrid assay, we observed that mutation of the Walker A motif of WRN had no effect on its ability to interact with WRNIP1 (Fig. 6B, panel a). In contrast, mutation of the Walker A motif of WRNIP1 abolished the interaction between WRN and WRNIP1 (Fig. 6B, panel b). This strongly suggested that the binding of ATP to WRNIP1, but not to WRN, is required for the association between WRN and WRNIP1.

We also observed evidence of self-association of WRNIP1 in the yeast two-hybrid assay when we used WRNIP1 as a bait (data not shown). To confirm the self-association of WRNIP1, FLAG-mWRNIP1 and HA-mWRNIP1 were co-expressed in human 293EBNA cells, and then subjected to immunoprecipitation using an anti-FLAG antibody. The proteins in the anti-FLAG immune complex were then analyzed by western blot using anti-FLAG or anti-HA antibodies. We observed that HA-mWRNIP1 was present in anti-FLAG immune complexes, indicating that mWRNIP1 self-associates in these cells (Fig. 6C).

To map the region of WRNIP1 responsible for self-association, we examined the ability of several WRNIP1 mutants to self-associate: it's a Zn finger domain mutant (23 Cys to Ser), a Walker A motif mutant (269 Lys to Ala), or a SRC domain mutant (366 Arg to Ala). Although the self-association of WRNIP1 was lightly attenuated by the Zn-finger mutation, none of the other mutants tested exhibited decreased levels of self-association (Fig. 6D).

## 4. Discussion

In this study, we generated DT40 mutant cell lines in which *WRNIP1*, *WRN*, or both genes were disrupted, in order to analyze the functional relationship of WRNIP1 and WRN. When we examined growth rate, cell cycle distribution, SCE and drug sensitivity of these cell lines, we found no evidence of a functional relationship between WRN and WRNIP1. Our data suggests that WRNIP1 is not a component of WRN-dependent signaling pathways that resolve DNA lesions induced by chemicals used in this study.

Since *WRNIP1*$^{-/-/-}$ cells expressed low levels of WRNIP1 containing a 52 amino acid deletion, it seems likely that this cell line is not a true null mutant. However, the mutant cells exhibited several phenotypes, and the deletion mutant behaved like a functional null mutant in yeast cells. Thus, we can claim that the deletion mutant at least behaves as a hypomorphic one. Notably, while *S. cerevisiae mgs1/sgs1* double mutant yeast exhibited an extremely severe defect in growth [23], *WRNIP1*$^{-/-/-}$/*WRN*$^{-/-}$ DT40 double mutant cells grew at the same rate as wild-type cells. This may be due to the fact that Sgs1 is the only RecQ helicase in budding yeast cells, while human and chicken cells have four additional RecQ helicases besides WRN [25]. Thus, it is possible that redundancy among vertebrate RecQ helicases rescues the growth defect caused by the deficiency of WRN in *WRNIP1*$^{-/-/-}$ cells.

On the other hand, *WRNIP1*$^{-/-/-}$/*WRN*$^{-/-}$ DT40 cells exhibited an additive increase in the frequency of SCE (Fig. 3B). This may reflect augmented defects in DNA replication that would normally be resolved through the homologous recombination pathway. In this context, the increase in SCE suggests that the hyper-recombination phenotype of *mgs1 sgs1* double mutant yeast [17,23] was mimicked in higher eukaryotic cells bearing mutations in *WRNIP1* and *WRN*.

We did not uncover functional evidence for cooperation between WRNIP1 and WRN following CPT exposure, raising the possibility that the physical association between WRNIP1 and WRN is not biologically relevant to recovery from CPT exposure. However, this does not necessarily exclude the possibility that WRNIP1 and WRN function cooperatively to resolve other types of DNA lesions. WRN interacts with dozens of proteins involved in DNA replication, repair, and recombination. Based on our previous results showing that only a small portion of endogenous WRN co-immunoprecipitated with endogenous WRNIP1 [16], it seems likely that cooperation of WRN and WRNIP1 is restricted to certain aspects of DNA metabolism, and the experimental condition used in this study are not suitable for examining the cooperative function of these two proteins. We believe the association of WRN and WRNIP1 reflects an authentic cellular interaction, based

on several lines of evidence that these proteins also interact with Fen1 and DNA polymerase δ (Polδ), both of which are involved in synthesis and maturation of Okazaki fragments in DNA replication. First, genetic studies in budding yeast indicated that Mgs1 interacts with Fen1 as well as Polδ [19,26]; second, purified hWRNIP1 interacted physically with human Polδ and stimulated loading of Polδ onto the template-primer in DNA synthesis (but did not stimulate processivity) either with or without PCNA [21]; third, in budding yeast, Mgs1 stimulated the activity of Fen-1 in an ATP-dependent manner *in vitro* [26]; and fourth, WRN has been shown interact physically with DNA polymerase δ [20], and stimulate the activity of DNA polymerase δ [13]. Finally, hWRN interacted with the C-terminal region of FEN-1 [27], and stimulated FEN-1 activity *in vitro* [14,27]. The results of the current study showed that WRNIP1 associated directly with WRN in an ATP-dependent manner. Reconstitution experiments examining the interplay of WRNIP1, WRN, FEN1, Polδ, as well as another replication proteins, such as PCNA, RFC, RPA, in the presence of ATP *in vitro*, will provide important clues to the biological role of the WRNIP1–WRN interaction.

One of potential mechanisms for the modulation of Polδ activity by WRN and WRNIP1 might be as follows. First, WRNIP1 in the ATP-bound state binds to a complex containing Polδ and WRN on the DNA replication fork. During the normal progression of DNA replication, WRN disrupts obstructive secondary structures of DNA around the replication fork, thereby supporting DNA synthesis mediated by Polδ. When DNA synthesis halts at a lesion on the template DNA, Polδ is released from the DNA replication intermediate, and WRNIP1 subsequently binds to the end of a nascent strand that is annealed to the template DNA [17]. The ATPase activity of hWRNIP1 was stimulated by template-primer DNA, but not by single-stranded or double-stranded DNA [21], suggesting that the template-primer DNA structure stimulates the ATPase activity of WRNIP1. Hydrolysis of ATP releases WRNIP1 from WRN, thereby permitting WRNIP1 to recruit Polδ to the replication fork, resulting in the resumption of DNA replication.

## Acknowledgments

This work was supported by Grants-in-Aid for Scientific Research and for Scientific Research on Priority Areas from the Ministry of Education, Culture, Sports, Science and Technology of Japan, and by Health Sciences Research Grants from the Ministry of Health, Labor and Welfare of Japan.

## Appendix A. Supplementary data

Supplementary data associated with this article can be found, in the online version, at doi:10.1016/j.dnarep.2006.04.006.

REFERENCES

[1] C.J. Epstein, G.M. Martin, A.L. Schultz, A.G. Motulsky, Werner's syndrome a review of its symptomatology, natural history, pathologic features, genetics and relationship to the natural aging process, Medicine (Baltimore) 45 (1966) 177–221.
[2] G.M. Martin, Cellular aging—clonal senescence. A review (Part I), Am. J. Pathol. 89 (1977) 484–511.
[3] K. Fukuchi, G.M. Martin, R.J. Monnat Jr., Mutator phenotype of Werner syndrome is characterized by extensive deletions, Proc. Natl. Acad. Sci. U.S.A. 86 (1989) 5893–5897.
[4] Y. Fujiwara, T. Higashikawa, M. Tatsumi, A retarded rate of DNA replication and normal level of DNA repair in Werner's syndrome fibroblasts in culture, J. Cell Physiol. 92 (1977) 365–374.
[5] R.M. Brosh Jr., V.A. Bohr, Roles of the Werner syndrome protein in pathways required for maintenance of genome stability, Exp. Gerontol. 37 (2002) 491–506.
[6] C.E. Yu, J. Oshima, Y.H. Fu, E.M. Wijsman, F. Hisama, R. Alisch, S. Matthews, J. Nakura, T. Miki, G.M. Martin, J. Mulligan, G.D. Schellenberg, Positional cloning of the Werner's syndrome gene, Science 272 (1996) 258–262.
[7] N. Suzuki, A. Shimamoto, O. Imamura, J. Kuromitsu, S. Kitao, M. Goto, Y. Furuichi, DNA helicase activity in Werner's syndrome gene product synthesized in a baculovirus system, Nucleic Acids Res. 25 (1997) 2973–2978.
[8] M.D. Gray, J.C. Shen, A.S. Kamath-Loeb, A. Blank, B.L. Sopher, G.M. Martin, J. Oshima, L.A. Loeb, The Werner syndrome protein is a DNA helicase, Nat. Genet. 17 (1997) 100–103.
[9] S. Huang, B. Li, M.D. Gray, J. Oshima, I.S. Mian, J. Campisi, The premature ageing syndrome protein, WRN, is a 3′→5′ exonuclease, Nat. Genet. 20 (1998) 114–116.
[10] N. Suzuki, M. Shiratori, M. Goto, Y. Furuichi, Werner syndrome helicase contains a 5′→3′ exonuclease activity that digests DNA and RNA strands in DNA/DNA and RNA/DNA duplexes dependent on unwinding, Nucleic Acids Res. 27 (1999) 2361–2368.
[11] L. Crabbe, R.E. Verdun, C.I. Haggblom, J. Karlseder, Defective telomere lagging strand synthesis in cells lacking WRN helicase activity, Science 306 (2004) 1951–1953.
[12] X. Du, J. Shen, N. Kugan, E.E. Furth, D.B. Lombard, C. Cheung, S. Pak, G. Luo, R.J. Pignolo, R.A. DePinho, L. Guarente, F.B. Johnson, Telomere shortening exposes functions for the mouse Werner and Bloom syndrome genes, Mol. Cell. Biol. 24 (2004) 8437–8446.
[13] A.S. Kamath-Loeb, E. Johansson, P.M. Burgers, L.A. Loeb, Functional interaction between the Werner syndrome protein and DNA polymerase delta, Proc. Natl. Acad. Sci. U.S.A. 97 (2000) 4603–4608.
[14] R.M. Brosh Jr., C. von Kobbe, J.A. Sommers, P. Karmakar, P.L. Opresko, J. Pitrowski, I. Dianova, G.L. Dianov, V.A. Bohr, Werner syndrome protein interacts with human flap endonuclease 1 and stimulates its cleavage activity, EMBO J. 20 (2001) 5791–5801.
[15] M.P. Cooper, A. Machwe, D.K. Orren, R.M. Brosh, D. Ramsden, V.A. Bohr, Ku complex interacts with and stimulates the Werner protein, Genes Dev. 14 (2000) 907–912.
[16] Y. Kawabe, D. Branzei, T. Hayashi, H. Suzuki, T. Masuko, F. Onoda, S.J. Heo, H. Ikeda, A. Shimamoto, Y. Furuichi, M. Seki, T. Enomoto, A novel protein interacts with the Werner's syndrome gene product physically and functionally, J. Biol. Chem. 276 (2001) 20364–20369.
[17] T. Hishida, H. Iwasaki, T. Ohno, T. Morishita, H. Shinagawa, A yeast gene, MGS1, encoding a DNA-dependent AAA(+) ATPase is required to maintain genome stability, Proc. Natl. Acad. Sci. U.S.A. 98 (2001) 8283–8289.
[18] T. Hishida, T. Ohno, H. Iwasaki, H. Shinagawa, *Saccharomyces cerevisiae MGS1* is essential in strains deficient in the *RAD6*-dependent DNA damage tolerance pathway, EMBO J. 21 (2002) 2019–2029.

[19] D. Branzei, M. Seki, F. Onoda, T. Enomoto, The product of *Saccharomyces cerevisiae WHIP/MGS1*, a gene related to replication factor C genes, interacts functionally with DNA polymerase delta, Mol. Genet. Genom. 268 (2002) 371–386.
[20] A.M. Szekely, Y.H. Chen, C. Zhang, J. Oshima, S.M. Weissman, Werner protein recruits DNA polymerase delta to the nucleolus, Proc. Natl. Acad. Sci. U.S.A. 97 (2000) 11365–11370.
[21] T. Tsurimoto, A. Shinozaki, M. Yano, M. Seki, T. Enomoto, Human Werner helicase interacting protein 1 (WRNIP1) functions as a novel modulator for DNA polymerase delta, Genes Cells 10 (2005) 13–22.
[22] O. Imamura, K. Fujita, C. Itoh, S. Takeda, Y. Furuichi, T. Matsumoto, Werner and Bloom helicases are involved in DNA repair in a complementary fashion, Oncogene 21 (2002) 954–963.
[23] D. Branzei, M. Seki, F. Onoda, H. Yagi, Y. Kawabe, T. Enomoto, Characterization of the slow-growth phenotype of *S. cerevisiae whip/mgs1 sgs1* double deletion mutants, DNA Repair (Amst) 1 (2002) 671–682.
[24] Y. Kawabe, M. Seki, T. Seki, W.S. Weng, O. Imamura, Y. Furuichi, H. Saitoh, T. Enomoto, Covalent modification of the Werner's syndrome gene product with the ubiquitin-related protein, SUMO-1, J. Biol. Chem. 275 (2000) 20963–20966.
[25] T. Enomoto, Functions of RecQ family helicases: possible involvement of Bloom's and Werner's syndrome gene products in guarding genome integrity during DNA replication, J. Biochem. (Tokyo) 129 (2001) 501–507.
[26] J.H. Kim, Y.H. Kang, H.J. Kang, D.H. Kim, G.H. Ryu, M.J. Kang, Y.s. Seo, *In vivo* and *in vitro* studies of Mgs1 suggest a link between genome instability and Okazaki fragment processing, Nucleic Acids Res. 33 (2005) 6137–6150.
[27] S. Sharma, J.A. Sommers, R.K. Gary, E. Friedrich-Heineken, U. Hubscher, R.M. Brosh Jr., The interaction site of Flap endonuclease-1 with WRN helicase suggests a coordination of WRN and PCNA, Nucleic Acids Res. 33 (2005) 6769–6781.

*Respirology* (2006) **11**, 826–829 doi: 10.1111/j.1440-1843.2006.00925.x

CASE REPORT

# Epithelioid sarcoma presenting as pulmonary cysts with cancer antigen 125 expression

EIKI KIKUCHI,[1] ICHIRO KINOSHITA,[2] KOICHI YAMAZAKI,[1] TOMOO ITOH,[3] TADAMICHI SHIMIZU,[4] HIROSHI SHIMIZU[4] AND MASAHARU NISHIMURA[1]

[1]*First Department of Medicine and* [4]*Department of Dermatology, Hokkaido University School of Medicine,* [2]*Department of Medical Oncology, Hokkaido University Graduate School of Medicine and* [3]*Department of Surgical Pathology, Hokkaido University Hospital, Sapporo, Japan*

**Epithelioid sarcoma presenting as pulmonary cysts with cancer antigen 125 expression**
KIKUCHI E, KINOSHITA I, YAMAZAKI K, ITOH T, SHIMIZU T, SHIMIZU H, NISHIMURA M. *Respirology* 2006; **11**: 826–829

**Abstract:** A 39-year-old Japanese woman presented with a swollen right hand and a right-sided pneumothorax. Chest CT revealed bilateral multiple pulmonary thin-walled cysts measuring ≤1 cm in diameter and small nodules. An initial skin biopsy led to a misdiagnosis of metastatic adenocarcinoma, as tumour cells were positive for cytokeratin, epithelial membrane antigen, carcinoembryonic antigen and cancer antigen 125. However, chemotherapy proved ineffective, and the skin biopsy was repeated. A final diagnosis of epithelioid sarcoma (ES) was made. Open lung biopsy showed that the pulmonary nodules represented metastases of ES. Although the pulmonary cyst walls did not contain tumour cells, bronchiolar wall adjacent to the cysts had been infiltrated by tumour cells. These findings suggested that pulmonary cysts, a rare form of pulmonary metastases from soft tissue sarcomas, had developed through a ball-valve effect of metastatic tumour in small airways. However, presence of cancer antigen 125 hindered obtaining a correct diagnosis of ES.

**Key words:** cancer antigen 125, epithelioid sarcoma, immunohistochemistry, pneumothorax, pulmonary cyst, pulmonary metastasis.

## INTRODUCTION

Epithelioid sarcoma (ES) is a rare soft-tissue sarcoma simulating necrotizing granuloma or carcinoma histologically and immunohistochemically. We describe a patient with ES and pulmonary metastases who presented with multiple pulmonary cysts with positive immunohistochemistry for cancer antigen 125 (CA125) leading to a misdiagnosis of adenocarcinoma of unknown primary site. Histopathological studies revealed the possible mechanism by which cystic pulmonary metastases may have developed.

Correspondence: Eiki Kikuchi, First Department of Medicine, Hokkaido University School of Medicine, North 15, West 7, Kitaku, Sapporo 060-8638, Japan. Email: eikik@med.hokudai.ac.jp

Received 3 July 2005; invited to revise 5 August 2005; revised 16 September 2005; accepted 6 October 2005 (Associate Editor: Toshihiro Nukiwa).



## CASE REPORT

A 39-year-old Japanese woman presented with a swollen the right hand that had gradually progressed to involve the forearm over the course of 15 months. An initial skin biopsy revealed nodular aggregates of epithelioid atypical cells with positive staining for cytokeratin, epithelial membrane antigen (EMA), carcinoembryonic antigen (CEA) and CA125. Metastatic carcinoma was suspected from the pathological examination. At the same time, the patient experienced a right-sided pneumothorax that required a chest tube drainage. Following lung reinflation a chest CT revealed bilateral multiple thin-walled pulmonary cysts ≤1 cm in diameter and multiple small nodules ≤5 mm in diameter, which were interpreted as pulmonary metastases (Fig. 1). Laboratory assessments were normal except for an elevated serum CA125 of 42.3 U/mL (normal: <35 U/mL), which supported a diagnosis of adenocarcinoma. However, systemic examination failed to reveal a primary site. Chemotherapy with carboplatin and paclitaxel was

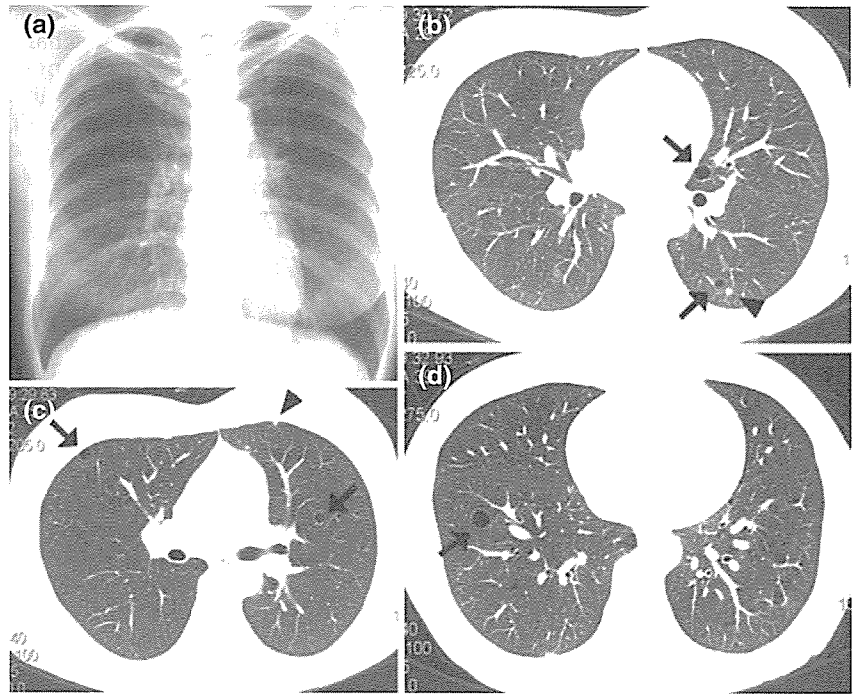


**Figure 1** (a) Patient's CXR showing no abnormalities. (b–d) CHEST CT showing bilateral multiple pulmonary thin-walled cysts ≤1 cm in diameter (arrows) and multiple small nodules ≤5 mm in diameter (arrowheads).

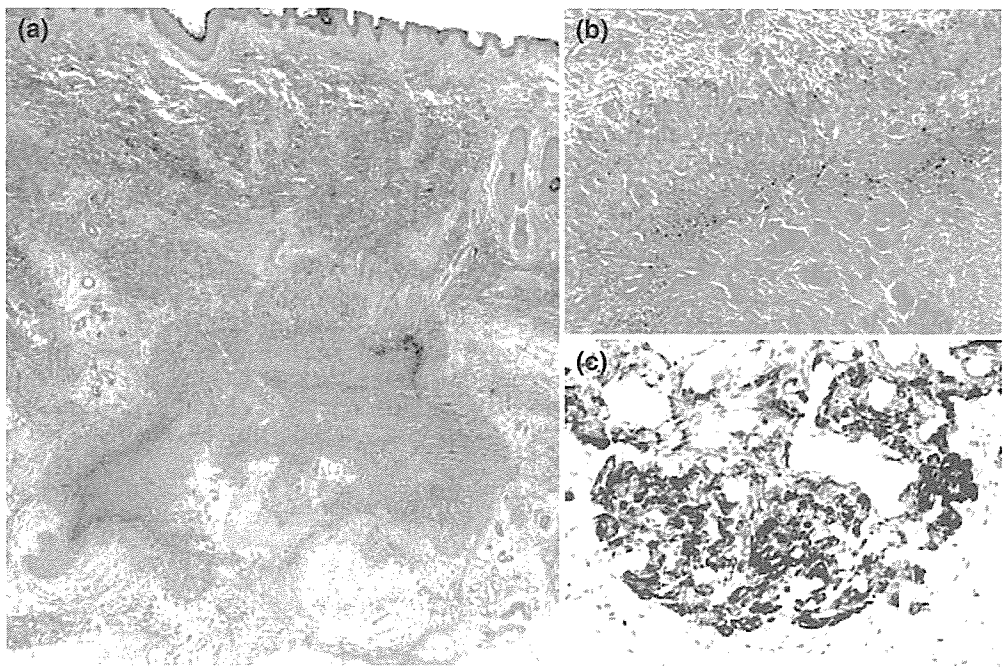


**Figure 2** (a) Skin biopsy specimen. The tumour was located in the lower dermis, showing geographic necrosis surrounded by epithelioid tumour cells with eosinophilic cytoplasm. These findings are typical for epithelioid sarcoma (×4, HE). (b) Epithelioid cells surrounded by collagenous stroma in a tumour with necrosis (×20, HE). (c) Tumour cells were strongly positive for CA125 (×40).

administered i.v. based on a diagnosis of metastatic adenocarcinoma of unknown origin. After chemotherapy, the swelling in the right hand did not change and the chest CT showed no marked changes in pulmonary cysts or nodules.

Biopsy from the skin of the right forearm was performed again 6 months after chemotherapy. Histopathological analysis showed epithelioid cells arranged in nodular aggregates around areas of central necrosis, which were typical for ES (Fig. 2a,b).

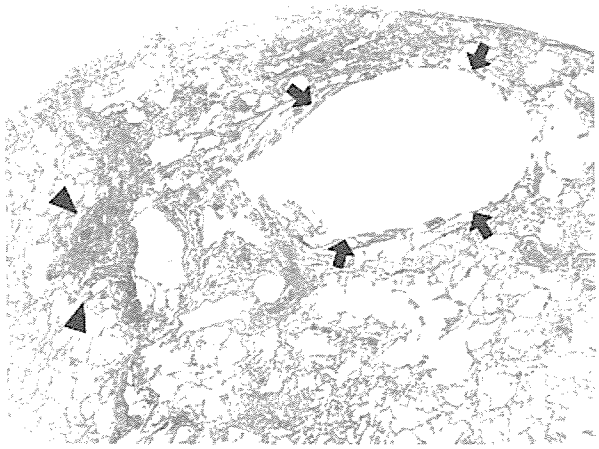

**Figure 3** Microscopic findings from the lung biopsy specimen showing that the cyst wall (arrows) contains no neoplastic cell component, but the wall of a small airway next to a cyst (arrowheads) contains malignant cells (×4, HE).

Immunohistochemical studies were performed again, revealing cells positive for vimentin in addition to cytokeratin, EMA, CEA and CA125 (Fig. 2c). ES of the right forearm was finally diagnosed. Open lung biopsy was performed to diagnose whether pulmonary cysts and nodules represented metastatic lesions. The pulmonary nodules consisted of epithelioid cells that were also positive for cytokeratin, EMA, CEA, CA125 and vimentin, and were thus diagnosed as metastases of ES. Pulmonary cysts contained air and were surrounded by normal lung parenchyma with no identifiable neoplastic cell component. However, the wall of a small airway next to a cyst contained malignant cells, suggesting that cysts developed as a result of a ball-valve effect of the metastatic tumour (Fig. 3).

The patient underwent chemotherapy for soft tissue sarcoma with ifosfamide, doxorubicin and cyclophosphamide in combination, resulting in no significant change. Thereafter she suffered from repeated bilateral pneumothorax, and died 53 months after she first felt swelling in the right hand.

## DISCUSSION

Epithelioid sarcoma is a distinctive soft tissue neoplasm with a predilection for the distal extremities of young adults.[1] Typical examples contain admixtures of epithelioid and spindle cells that are often arranged in nodular aggregates around areas of central necrosis, simulating necrotizing granuloma or carcinoma. Metastases to the lymph nodes, lungs and skin reportedly occur in about 50% of patients with ES.[2,3] Pulmonary metastases of soft tissue sarcomas commonly take the form of solid nodules. Although some tumours occasionally present as cystic pulmonary metastases, few cases of cystic pulmonary metastases of soft tissue sarcomas have been described.[4,5] Three possible mechanisms have been proposed for the development of malignant cysts:[4–6] (i) excavation of a nodular tumour through discharge of the necrotic material inside; (ii) infiltration of malignant cells into the walls of a pre-existing benign pulmonary bulla; or (iii) distension of alveoli and small airways by partial bronchial obstruction through the ball-valve effect of the tumour. Involvements of the first and second mechanisms in our patient were ruled out due to the absence of identifiable neoplastic cells around cysts. The presence of malignant cells in the bronchiolar wall next to a cyst would suggest that the mechanism of development of the cyst in the present case was the ball-valve effect. Pneumothorax may therefore have also been caused by distension of alveoli through the ball-valve effect, permitting passage of air along the interlobular septa to the pleura, where blebs may have formed and eventually ruptured.

Immunohistochemical analyses of ES, typically reveal positive results for vimentin, keratins, EMA and occasionally CEA and CD34.[7] In this patient, tumour cells were positive for CA125 in addition to vimentin, keratin, EMA and CEA. CA125 is a large glycoprotein expressed on the epithelium of the fallopian tubes, endometrium, endocervix and ovary, in addition to mesothelial cells of the pleura, pericardium and peritoneum.[8] CA125 is a differentiation antigen associated with coelomic epithelium and both normal and neoplastic derivatives. Serum CA125 concentration has been found to represent a marker for epithelial ovarian carcinoma. CA125 is also reportedly elevated in other cancers, including endometrial, pancreatic, lung, breast and colon cancer. Elevated serum levels of CA125 have occasionally been reported in mesenchymal tumours such as leiomyosarcoma,[9] alveolar rhabdomyosarcoma[10] and desmoplastic small round cell tumour.[11] Kato *et al.* recently reported elevated levels of serum CA125 in three patients with ES, and immunohistochemical expression in 10 of 11 ES patients.[12,13] These patients in addition to the present patient suggest that CA125 might prove useful as an immunohistochemical and serum marker for diagnosing ES. Clinicians and pathologists should be aware of the possibility of ES when encountering cases with nodular aggregates of epithelioid atypical cells that are positive for CA125.

## REFERENCES

1 Enzinger FM. Epitheloid sarcoma. A sarcoma simulating a granuloma or a carcinoma. *Cancer* 1970; **26**: 1029–41.
2 Chase DR, Enzinger FM. Epithelioid sarcoma. Diagnosis, prognostic indicators, and treatment. *Am. J. Surg. Pathol.* 1985; **9**: 241–63.
3 Prat J, Woodruff JM, Marcove RC. Epithelioid sarcoma: an analysis of 22 cases indicating the prognostic significance of vascular invasion and regional lymph node metastasis. *Cancer* 1978; **41**: 1472–87.
4 Traweek T, Rotter AJ, Swartz W, Azumi N. Cystic pulmonary metastatic sarcoma. *Cancer* 1990; **65**: 1805–11.
5 Hasegawa S, Inui K, Kamakari K, Kotoura Y, Suzuki K, Fukumoto M. Pulmonary cysts as the sole metastatic

manifestation of soft tissue sarcoma: case report and consideration of the pathogenesis. *Chest* 1999; **116**: 263–5.
6 Anderson HJ, Pierce JW. Carcinoma of bronchus presenting as thin walled cysts. *Thorax* 1954; **91**: 100–5.
7 Miettinen M, Fanburg-Smith JC, Virolainen M, Shmookler BM, Fetsch JF. Epithelioid sarcoma: an immunohistochemical analysis of 112 classical and variant cases and a discussion of the differential diagnosis. *Hum. Pathol.* 1999; **30**: 934–42.
8 Niloff JM, Knapp RC, Schaetzl E, Reynolds C, Bast RC Jr. CA125 antigen levels in obstetric and gynecologic patients. *Obstet. Gynecol.* 1984; **64**: 703–7.
9 Whiteley MS, Marshall J. Raised serum CA125 level in leiomyoma and leiomyosarcoma of gastrointestinal origin. *Br. J. Surg.* 1993; **80**: 1551.
10 Holcomb K, Francis M, Ruiz J, Abulafia O, Matthews RP, Lee YC. Pleomorphic rhabdomyosarcoma of the uterus in a postmenopausal woman with elevated serum CA125. *Gynecol. Oncol.* 1999; **74**: 499–501.
11 Ordóñez NG, Sahin AA. CA 125 production in desmoplastic small round cell tumor: report of a case with elevated serum levels and prominent signet ring morphology. *Hum. Pathol.* 1998; **29**: 294–9.
12 Kato H, Hatori M, Kokubun S *et al.* CA125 expression in epithelioid sarcoma. *Jpn. J. Clin. Oncol.* 2004; **34**: 149–54.
13 Kato H, Hatori M, Watanabe M, Kokubun S. Epithelioid sarcomas with elevated serum CA125: report of two cases. *Jpn. J. Clin. Oncol.* 2003; **33**: 141–4.

Graefe's Arch Clin Exp Ophthalmol
DOI 10.1007/s00417-005-0168-3

CLINICAL INVESTIGATION

Nobuyoshi Kitaichi
Tadamichi Shimizu
Ayumi Honda
Riichiro Abe
Kazuhiro Ohgami
Kenji Shiratori
Hiroshi Shimizu
Shigeaki Ohno

# Increase in macrophage migration inhibitory factor levels in lacrimal fluid of patients with severe atopic dermatitis

Received: 28 April 2005
Revised: 17 September 2005
Accepted: 18 September 2005


N. Kitaichi (✉) · K. Ohgami · K. Shiratori · S. Ohno
Department of Ophthalmology and Visual Sciences, Hokkaido University Graduate School of Medicine, 060-8638, Sapporo, Japan
e-mail: nobukita@med.hokudai.ac.jp

T. Shimizu · A. Honda · R. Abe · H. Shimizu
Department of Dermatology, Hokkaido University Graduate School of Medicine, 060-8638, Sapporo, Japan

**Abstract** *Background and aims of the study:* Atopic dermatitis is a chronic inflammatory skin disorder that often involves some ophthalmic features. Macrophage migration inhibitory factor (MIF) is a proinflammatory cytokine that is associated with the generation of cell-mediated immune responses. Although serum MIF levels may be elevated in severe atopic dermatitis, the quantity of MIF in regional ocular fluid remains unknown. We measured MIF levels in tears (lacrimal fluid) of patients with atopic dermatitis. *Patients and methods:* Tear samples were collected from 16 patients with atopic dermatitis, 10 patients with allergic conjunctivitis, and 15 healthy control subjects. The clinical severity of atopic dermatitis was evaluated according to the Scoring Atopic Dermatitis (SCORAD) index. The index was calculated by summing the following scores: extent criteria, intensity criteria, and subjective symptoms. Macrophage migration inhibitory factor levels were determined by a human MIF enzyme-linked immunosorbent assay. All comparisons were two-tailed, and $P$ values $<0.01$ were considered as statistically significant. *Results:* The mean MIF concentration in lacrimal fluid collected from healthy control subjects was 0.69± 0.2 ng/ml. The mean tear MIF levels were 17.87± 6.3 ng/ml in moderate-to-severe atopic dermatitis (SCORAD≥ 15, $P$=0.002), 0.93±0.08 ng/ml in mild atopic dermatitis (SCORAD< 15), and 2.76± 0.86 ng/ml in allergic conjunctivitis ($P$=0.008). *Conclusions:* A proinflammatory cytokine MIF level was elevated in tears as well as serum in cases of severe atopic dermatitis. These results suggest that MIF may play an important role in the induction or enhancement of ophthalmic features related to severe atopic dermatitis.

**Keywords** Allergic conjunctivitis · Atopic dermatitis · Eye · MIF · Serum · Tears

## Introduction

Macrophage migration inhibitory factor (MIF) was first discovered in the late 1960s; it is therefore believed to be the first recognized lymphokine [6]. Since MIF was discovered as merely a part of the phenomenon of inhibiting migration of macrophages in the pre-molecular biology era, many scientists doubted its importance in the immune response. Investigations in the 1990s aimed at identifying novel systemic mediators that could regulate host inflammatory responses led to the identification of murine MIF as a product secreted by the anterior pituitary gland [2]. Upon stimulation, T cells release MIF, and MIF activity was first described as a product of cognate T-cell supernatants [15]. Macrophages have also been identified as an important source of MIF and are known to express MIF both constitutively and upon stimulation [15]. Macrophage migration inhibitory factor is considered to act by both paracrine and autocrine stimulatory pathways to augment the activation of these cells [15]. As reported